Efficient Measurement of Quantum Dynamics via Compressive Sensing

A. Shabani,[1] R. L. Kosut,[2] M. Mohseni,[3] H. Rabitz,[1] M. A. Broome,[4] M. P. Almeida,[4] A. Fedrizzi,[4] and A. G. White[4]

[1]*Department of Chemistry, Princeton University, Princeton, New Jersey 08544, USA*
[2]*SC Solutions, Sunnyvale, California 94085, USA*
[3]*Research Laboratory of Electronics, Massachusetts Institute of Technology, Cambridge, Massachusetts 02139, USA*
[4]*Center for Engineered Quantum Systems and Center for Quantum Computation and Communication Technology, School of Mathematics and Physics, The University of Queensland, QLD 4072, Australia*

(Received 5 November 2009; revised manuscript received 14 November 2010; published 7 March 2011)

The resources required to characterize the dynamics of engineered quantum systems—such as quantum computers and quantum sensors—grow exponentially with system size. Here we adapt techniques from compressive sensing to exponentially reduce the experimental configurations required for quantum process tomography. Our method is applicable to processes that are nearly sparse in a certain basis and can be implemented using only single-body preparations and measurements. We perform efficient, high-fidelity estimation of process matrices of a photonic two-qubit logic gate. The database is obtained under various decoherence strengths. Our technique is both accurate and noise robust, thus removing a key roadblock to the development and scaling of quantum technologies.

DOI: 10.1103/PhysRevLett.106.100401 PACS numbers: 03.65.Wj, 03.65.Yz, 03.67.Lx

Understanding and controlling the world at the nanoscale—be it in biological, chemical or physical phenomena—requires quantum mechanics. It is therefore essential to characterize and monitor realistic complex quantum systems that inevitably interact with typically uncontrollable environments. One of the most general descriptions of the dynamics of an open quantum system is a quantum map—typically represented by a process matrix [1]. Methods to identify this matrix are collectively known as quantum process tomography (QPT) [1,2]. For a d-dimensional quantum system, they require $O(d^4)$ experimental configurations: combinations of input states, on which the process acts, and a set of output observables. For a system of n qubits—two level quantum systems—$d = 2^n$. The required physical resources hence scale exponentially with system size. Recently, a number of alternative methods have been developed for efficient and selective estimation of quantum processes [3]. However, full characterization of quantum dynamics of comparably small systems, such as an 8-qubit ion trap [4], would still require over a billion experimental configurations, clearly impractical. So far, process tomography has therefore been limited by experimental and off-line computational resources, to systems of 2 and 3 qubits [5–7].

Here we adapt techniques from compressive sensing to develop an experimentally efficient method for QPT. It requires only $O(s \log d)$ configurations if the process matrix is s compressible in some known basis, i.e., it is nearly sparse in that it can be well approximated by an s-sparse process matrix. This is usually the case, because engineered quantum systems aim to implement a unitary process which is maximally sparse in its eigenbasis. In practice, as observed in liquid-state NMR [8], photonics [5,9,10], ion traps [11], and superconducting circuits [6], a near-unitary process will still be nearly sparse in this basis, and still compressible. The near sparsity is due to few dominant system environment interactions. This is more apparent for weakly decohering systems [12].

We experimentally demonstrate our algorithm by estimating the 240 real parameters of the process matrix of a canonical photonic two-qubit gate, Fig. 1, from a reduced number of configurations. From just 18 and 32 configurations, we obtain fidelities of 94% and 97% with process matrices obtained from an overcomplete set of all 576 available configurations.

Compressive sensing provides methods for compression of information carried by a large-size signal into a significantly smaller one along with efficient convex optimization algorithms to decipher this information [13]. Originally developed to exploit compressible features of

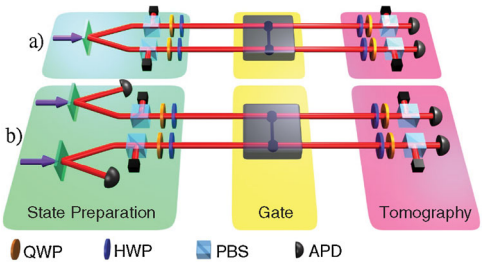

FIG. 1 (color online). Experimental scheme. Two-photon inputs were prepared with either (a) a high-rate, nonscalable, two-photon source or (b) a low-rate, scalable, four-photon source. The qubits are encoded using polarization, as described in the text. The quantum process is a photonic entangling gate. A measurement configuration is defined as some combination of state preparation and an observable, implemented here with quarter- and half-wave plates (QWP, HWP), polarizers (PBS), and photon detectors (APD). For details see [19].

audio and video signals, compressive sensing is now applied to: simulations of compressive sensing for QPT [14], ghost imaging [15], and state tomography for low-rank density matrices [16]. The latter provides a quadratic reduction of physical resources from d^2 for standard tomography to $O(rd\log^2 d)$ for a density matrix of rank r with the added advantage that rank is basis independent. Recently, this method has been useful in efficient state tomography of one-dimensional systems approximated by matrix product states [17].

Under reasonable assumptions, a quantum map on a d-dimensional space has the general representation [1],

$$\mathcal{S}(\rho) = \sum_{\alpha,\beta=1}^{d^2} \chi_{\alpha\beta}\Gamma_\alpha \rho \Gamma_\beta^\dagger \tag{1}$$

where χ, the $d^2 \times d^2$ process matrix, is positive semidefinite, $\chi \geq 0$, and trace preserving, $\sum_{\alpha,\beta}\chi_{\alpha\beta}\Gamma_\beta^\dagger\Gamma_\alpha = I_d$, with $\{\Gamma_\alpha\}$ an orthonormal matrix basis set, $\mathrm{Tr}(\Gamma_\beta^\dagger\Gamma_\alpha) = \delta_{\alpha\beta}$. Note that sparsity is a property of the map representation not the map itself. Data is collected by preparing an ensemble of identical systems in one of the states $\{\rho_1, \ldots, \rho_k\}$, inputting them to the process χ, and then measuring an observable M from the set $\{M_1, \ldots, M_\ell\}$. For a pair (ρ, M), the outcome will be $y_{M,\rho} = \mathrm{Tr}(\mathcal{S}(\rho)M)$. If the experiment is repeated for all configurations, i.e., (ρ_i, M_i), $i = 1, \ldots, m = k\ell$, the relation between the vector of outcomes $y = [y_{M_1,\rho_1}, \ldots, y_{M_m,\rho_m}]^T$ and the true process matrix, denoted by χ_0, can be represented by a linear map $y = \Phi\vec{\chi}_0$, where $\vec{\chi}_0$ is the vectorized form of the process matrix χ_0 and Φ is an $m \times d^4$ matrix of coefficients of the form $\mathrm{Tr}(\Gamma_\alpha\rho_i\Gamma_\beta^\dagger M_i)/\sqrt{m}$.

In general, estimating a sparse process matrix with an unknown sparsity pattern from an underdetermined set of linear equations ($m < d^4$) would seem highly unlikely. Compressive sensing, however, tells us that this can be done by solving for χ from the convex optimization problem:

$$\text{minimize } \|\vec{\chi}\|_{\ell_1} \text{ subject to } \|y - \Phi\vec{\chi}\|_{\ell_2} \leq \varepsilon, \tag{2}$$

and positive-semidefinite and trace-preserving conditions as defined above. The parameter ε quantifies the level of uncertainty in the measurements, that is, we observe $y = \Phi\chi_0 + w$ with $\|w\|_{\ell_2} \leq \varepsilon$. From [18], recovery via (2) is ensured if (i) the matrix Φ satisfies the restricted isometry property:

$$1 - \delta_s \leq \frac{\|\Phi\vec{\chi}_1(s) - \Phi\vec{\chi}_2(s)\|_{\ell_2}^2}{\|\vec{\chi}_1(s) - \vec{\chi}_2(s)\|_{\ell_2}^2} \leq 1 + \delta_s \tag{3}$$

for all s-sparse $\chi_1(s)$, $\chi_2(s)$ process matrices; (ii) the isometry constant $\delta_{2s} < \sqrt{2} - 1$ and (iii) the number of configurations $m \geq C_0 s\log(d^4/s)$. Under these conditions, the solution $\chi^\star$ of (2) satisfies,

$$\|\vec{\chi}^\star - \vec{\chi}_0\|_{\ell_2} \leq \frac{C_1}{\sqrt{s}}\|\vec{\chi}_0(s) - \vec{\chi}_0\|_{\ell_1} + C_2\varepsilon \tag{4}$$

where $\chi_0(s)$ is the best s-sparse approximation of χ_0 and C_0, C_1, C_2 are constants on the order of $O(\delta_s)$, see [19]. The restricted isometry property states that two s-sparse process matrices $\chi_1(s)$ and $\chi_2(s)$ can be distinguished if their relative distance is nearly preserved after the measurements. If the measurements are noise free, $\varepsilon = 0$, and χ_0 is s sparse, $\chi_0 = \chi_0(s)$, then the right-hand side of (4) is zero leading to perfect recovery, $\chi^\star = \chi_0$. Otherwise the solution tends to the best s-sparse approximation of the process matrix plus the additional term due to measurement error ε. If for an n-qubit QPT with $d = 2^n$ the conditions of the above analysis are satisfied, then the number of experimental configurations m scales linearly with sn, specifically, $m \geq C_0 s(4n\log 2 - \log s) = O(sn)$. In [19], using the measure concentration properties of random matrices, following the arguments in [20], we show that if Φ is constructed from random input states $\{\rho_i\}$, and random observables $\{M_i\}$, then the restricted isometry in (3) holds with high probability. Also a test is presented to certify the sparsity assumption.

A nearly sparse process matrix can be recovered from an exponentially smaller number of measurement outcomes to within the bounds of (4) by solving (2). We now test our algorithm experimentally against standard QPT on a two-qubit gate under a range of decoherence—and thus sparsity—conditions. We used a photonic controlled-phase, CZ, gate, Fig. 1 where the qubits are encoded in orthogonal polarization states of single photons ($|H\rangle$, horizontal, and $|V\rangle$, vertical). We performed full process tomography [5,9,10] of the gate with both two-photon and four-photon arrangements, preparing 16 pairwise combinations of the 4 input states $\{|H\rangle, |V\rangle, |D\rangle, |R\rangle\}$ and, for each input, measuring 36 two-qubit combinations of the observables $\{|H\rangle, |V\rangle, |D\rangle, |A\rangle, |R\rangle, |L\rangle\}$, where $|D(A)\rangle = (|H\rangle \pm |V\rangle)/\sqrt{2}$ and $|R(L)\rangle = (|H\rangle \pm i|V\rangle)/\sqrt{2}$. These 576 input-output configurations represent an overcomplete set which allows the best possible estimate of the quantum process, denoted χ_{576} [5].

The compressed quantum process tomography (CQPT) estimate of the 16×16 process matrix, χ_m, is obtained by solving (2) with $y = C_{\mathrm{sel}}p$ and $\Phi = C_{\mathrm{sel}}G$ where p is the vector of 576 experimental probabilities corresponding to each of the 576 configurations, G is the 576×256 matrix obtained from all the configurations with the basis set $\{\Gamma_\alpha\}$, and C_{sel} is the $m \times 576$ matrix corresponding to taking a selection of $m \leq 576$ of all possible configurations. The basis set is obtained from the singular-value decomposition of the ideal CZ gate: the process matrix in this basis is maximally sparse with a single nonzero (1, 1) element. The measurement error bound ε in (2) is chosen to be just slightly larger than $\sqrt{m}\sigma$, where σ is the minimum feasible root-mean-square level obtained from (2) using all configurations, i.e., with $C_{\mathrm{sel}} = I_{576}$. We quantify decoherence using the process purity, $\mathcal{P} = \mathrm{Tr}(\chi_m^2/d^2)$, which varies from 0 for a completely decohering channel, to 1 for a unitary process: in our experiment we used six

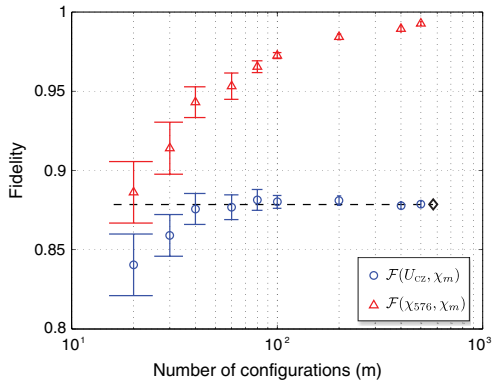

FIG. 2 (color online). Process fidelities vs number of input-output configurations, for each compressive QPT estimate, χ_m, in the gate basis of the ideal CZ gate for the lowest measured noise level, $\mathcal{P} = 0.91$. The dashed line shows the fidelity of the full estimate $\mathcal{F}(U_{cz}, \chi_{576}) = 0.89$ (black diamond). Error bars are obtained by solving (2) for 50 different random combinations of m inputs and observables.

decoherence levels (see [19] for details), giving purities of $\{0.62, 0.74, 0.77, 0.79, 0.86, 0.91\} \pm 0.01$.

Figure 2 shows, for the lowest decoherence level, the process fidelities [5] versus the number of randomly selected configurations, m. Each process matrix, $\{\chi_m\}$, is obtained by solving (2). We use the fidelity between (i) the compressive measurement and the ideal, $\mathcal{F}(U_{cz}, \chi_m)$; and (ii) the compressed and optimal measurements, $\mathcal{F}(\chi_{576}, \chi_m)$. Note that as m increases the fidelity with the ideal converges to the value of 0.89 obtained from χ_{576}; likewise, the fidelity with the full estimate converges to unity. Similar plots exist for every level of decoherence, with fidelities reduced accordingly.

We have so far used random selections of probabilities from the full data set, which allows us a comprehensive test of CQPT. Experiments, however, do not yield probabilities but physical quantities, e.g., count rates. To date, algorithms for more efficient state [16] or process tomography have assumed probabilities as a starting point. Since normalization is an issue to some extent in all physical architectures, it will be necessary to investigate the robustness and scalability of algorithms for real-world experiments.

For our photonic two-qubit gate, which is lossy and intrinsically probabilistic, the probabilities were obtained by normalizing counts using a full basis set of observables extracted from all measurements, I_{576}. Having sufficient configurations to allow for normalization necessarily imposes limits on CQPT efficiency: for low m, we are restricted in how random our selections can be. (Details and some permissible configurations in [19]). As an example, Fig. 3 shows process matrices reconstructed via CQPT from just one of these configurations compared to the respective full data estimates. We used 32 combinations of the 16 inputs $\{|H\rangle, |V\rangle, |D\rangle, |R\rangle\}^{\otimes 2}$ and 2 observables $\{|R\rangle|I\rangle, |I\rangle|R\rangle\}$, where I is the identity. The agreement is excellent as one can see from the fidelities and the correct reproduction of imaginary elements—which are ideally zero. Another striking feature is that we obtain highly faithful reconstructions of a nonlocal process using only local measurements [2].

A further crucial test is whether CQPT enables us to locate errors and implement necessary corrections: a common example is identifying local rotations that move the process closer to the ideal. By optimizing $\mathcal{F}(U_{cz}, \chi_{32})$, we calculated local corrections to χ_{32}; applying them to the full estimate χ_{576}, $\mathcal{F}(U_{cz}, \chi_{576})$ improved, on average, over all decoherence levels, by 4.1%. This is very close to the average 4.9% improvement obtained by calculating and applying local corrections *directly* to χ_{576}. Even a low-configuration CQPT estimate of a noisy process therefore enables improvements.

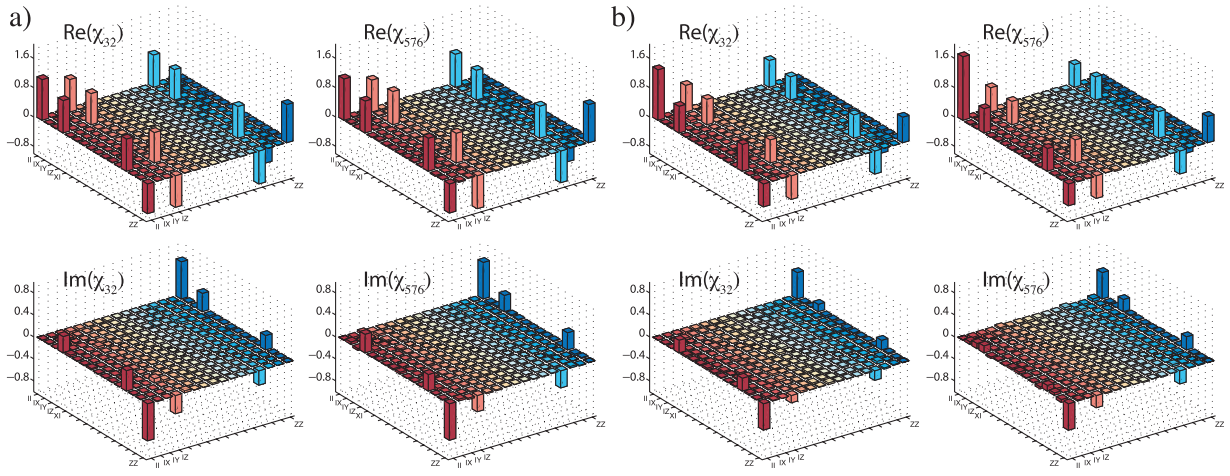

FIG. 3 (color online). Real and imaginary process matrix elements in the Pauli basis for the CQPT estimate χ_{32}, 32 configurations (left) vs full data estimate χ_{576}, 576 configurations (right) for (a) a low noise, two-photon experiment, $\mathcal{P} = 0.91$, and (b) a high-noise, four-photon experiment, $\mathcal{P} = 0.62$. The CQPT reconstructions have fidelities, $\mathcal{F}(\chi_{576}, \chi_{32})$, of 95% and 85%, respectively. The CQPT estimation accuracy is excellent for low noise, and reliable even for high noise, see [19] for more details.

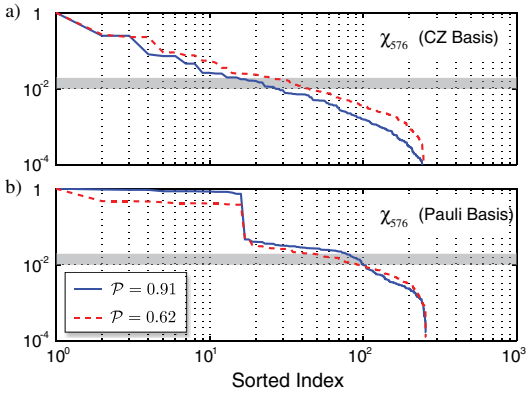

FIG. 4 (color online). Absolute values of the 256 process matrix elements of χ_{576} for our lowest and highest noise level, sorted by relative magnitude [with respect to the (1, 1) element] in the CZ basis (top) and the Pauli basis (bottom). The error threshold, which indicates the required number of configurations, is shown in grey.

That high-fidelity estimates are obtained by CQPT can be understood from the error bound (4) which shows that the CQPT estimate tends towards the best s-sparse approximation of the true process, χ_{576}. Figure 4 shows the process matrix elements, sorted by relative magnitude, for low- and high-noise levels, in two basis sets. The s-sparse approximation levels indicated in (4) are reached where the matrix elements drop below the error threshold (0.01–0.02). For the corresponding m, we can therefore expect a successful, high-fidelity, CQPT reconstruction. In the CZ basis, the plots show that for low noise, $s \in [20, 30]$, which correlates well with the fidelities in Fig. 2; for high noise $s \in [40, 60]$. Although the process matrix is still somewhat sparse in the Pauli basis (Fig. 3). Figure 4(b) indicates that ~100 configurations are needed to obtain an estimate of comparable quality. Furthermore, the sorted magnitude values in the CZ basis decay exponentially, which is sufficient to declare the process matrix s compressible, see, e.g., [21,22]. Intriguingly, this exponential decay is a signature of model-based compressive sensing where the scaling goes from $m = O(s \log(d/s))$ to $m = O(s)$ [22]. This demands further investigation, since it appears that QPT fits this framework, particularly when the process matrix is expanded in the ideal basis corresponding to the unitary design goal.

Our experimental results are supported numerically by simulations of a 2-qubit process as well as simulation studies for 3- and 4-qubit systems which show the same type of compressibility, see [19]. Applying CQPT to larger systems will require careful attention to classical postprocessing which—as in QPT—scales exponentially. The standard software we used here (see [19]), can easily handle 2- and 3-qubit CQPT systems. For larger systems, more specialized software can increase speed by orders of magnitude, see, e.g., [21].

A number of research directions arise from this work: incorporating knowledge of model structure properties; tightening the bounds on scaling laws; understanding how near-sparsity s and rank r vary with system dimension, d; pursuing highly efficient convex-computational algorithms; and selection of optimal configurations. Compressive tomography techniques can also be applied to quantum metrology and Hamiltonian parameter estimation: for example, estimating selective properties of biological or chemical interest in molecular systems and nanostructures with typically sparse Hamiltonians [23].

We thank J. Romberg and S. Jafarpour for discussions. We acknowledge funding by the ARC Discovery and Federation Fellowship programs and an IARPA-funded US Army Research Office contract. R. L. K. and H. R are supported by DARPA Grant No. FA9550-09-1-0710 administered through AFOSR.

[1] M. A. Nielsen and I. L. Chuang, *Quantum Computation and Quantum Information* (Cambridge University Press, Cambridge, UK, 2000).
[2] J. B. Altepeter *et al.*, Phys. Rev. Lett. **90**, 193601 (2003); M. Mohseni and D. Lidar, Phys. Rev. Lett. **97**, 170501 (2006); M. Lobino *et al.*, Science **322**, 563 (2008); M. Mohseni, A. T. Rezakhani, and D. A. Lidar, Phys. Rev. A **77**, 032322 (2008).
[3] J. Emerson *et al.*, Science **317**, 1893 (2007); A. Bendersky *et al.*, Phys. Rev. Lett. **100**, 190403 (2008); M. Branderhorst *et al.*, New J. Phys. **11**, 115010 (2009).
[4] H. Haffner *et al.*, Nature (London) **438**, 643 (2005).
[5] J. O'Brien *et al.*, Phys. Rev. Lett. **93**, 080502 (2004).
[6] R. Bialczak *et al.*, Nature Phys. **6**, 409 (2010).
[7] T. Monz *et al.*, Phys. Rev. Lett. **102**, 040501 (2009).
[8] A. M. Childs, I. L. Chuang, and D. W. Leung, Phys. Rev. A **64**, 012314 (2001); N. Boulant *et al.*, Phys. Rev. A **67**, 042322 (2003); Y. Weinstein *et al.*, J. Chem. Phys. **121**, 6117 (2004).
[9] M. W. Mitchell *et al.*, Phys. Rev. Lett. **91**, 120402 (2003).
[10] Y. Nambu and K. Nakamura, Phys. Rev. Lett. **94**, 010404 (2005).
[11] M. Riebe *et al.*, Phys. Rev. Lett. **97**, 220407 (2006).
[12] M. Mohseni and A. T. Rezakhani, Phys. Rev. A **80**, 010101 (2009); A. G. Kofman and A. N. Korotkov, Phys. Rev. A **80**, 042103 (2009).
[13] E. Candes and M. Wakin, IEEE Signal Process. Mag. **25**, 21 (2008).
[14] R. L. Kosut, arXiv:0812.4323v1.
[15] O. Katz *et al.*, Appl. Phys. Lett. **95**, 131110 (2009).
[16] D. Gross *et al.*, Phys. Rev. Lett. **105**, 150401 (2010).
[17] M. Cramer *et al.*, Nature Commun. **1**, 149 (2010).
[18] E. J. Candes, C.R. Seances Acad. Sci. Ser. 1 **346**, 589 (2008).
[19] See supplemental material at http://link.aps.org/supplemental/10.1103/PhysRevLett.106.100401.
[20] R. Baraniuk *et al.*, Constr. Aprox. **28**, 253 (2008).
[21] D. Needell and J. A. Tropp, Appl. Comput. Harmon. Anal. **26** 301 (2009).
[22] R. G. Baraniuk *et al.*, IEEE Trans. Inf. Theory **56**, 1982 (2010).
[23] J. Yuen-Zhou *et al.*, arXiv:1006.4866.